Chemical Engineering Journal 429 (2022) 132497

Contents lists available at ScienceDirect

Chemical Engineering Journal

journal homepage: www.elsevier.com/locate/cej

Photocatalytic Cr(VI) reduction over MIL-101(Fe)–NH_2 immobilized on alumina substrate: From batch test to continuous operation

Qian Zhao [a], Xiao-Hong Yi [a], Chong-Chen Wang [a,*], Peng Wang [a], Weiwei Zheng [b]

[a] Beijing Key Laboratory of Functional Materials for Building Structure and Environment Remediation/Beijing Energy Conservation & Sustainable Urban and Rural Development Provincial and Ministry Co-construction Collaboration Innovation Center, Beijing University of Civil Engineering and Architecture, Beijing 100044, PR China
[b] Department of Chemistry, Syracuse University, Syracuse, NY 13244, United States

ARTICLE INFO

Keywords:
MIL-101(Fe)–NH_2
Cr(VI) reduction
Fixed-bed reactor
Batch test
Continuous operation

ABSTRACT

MIL-101(Fe)–NH_2 was hydrothermally immobilized on porous alumina substrate to fabricate MIL-101(Fe)–NH_2@Al_2O_3 (MA) photocatalyst via a reactive seeding (RS) method. The as-prepared MA photocatalyst can accomplish 100% Cr(VI) reduction efficiency up to 20 cycles with the synergistic effect of oxalic acid upon the irradiation of white light. The influences of co-existing inorganic ions in simulated tanning wastewater on Cr(VI) reduction were evaluated via a Box-Behnken design of response surface methodology. The as-prepared MA photocatalyst can overcome the difficulty and challenge concerning the recovery and recyclability of traditional powder MOFs photocatalysts. Furthermore, a continuous fixed-bed device based on MA photocatalyst was designed, which can achieve a rapid and efficient Cr(VI) reduction under white light in lab experiment and under the real solar light in field experiment. This work provides the possibility for the continuous photocatalytic Cr (VI) reduction operation in the fixed-bed reactor.

1. Introduction

Hexavalent chromium (Cr(VI)), usually as the form of $Cr_2O_7^{2-}$, is a widespread contaminant in wastewaters discharged from various industrial processes like electroplating, pigment production, and leather tanning [1,2]. Due to its high toxicity, strong carcinogenicity, and high solubility, the World Health Organization (WHO) set a stricter threshold of 50 μg/L for Cr(VI) (in drinking water) [3]. A variety of strategies have been adopted for the treatment of Cr(VI) containing wastewater, including ion exchange [4], adsorption [5], chemical or electrochemical reduction [6], membrane filtration [7]. Among these elimination technologies, the photocatalytic Cr(VI) reduction into Cr(III) is well-acknowledged as an effective Cr(VI) removal method. Many researchers have reported the photocatalytic Cr(VI) reduction over different photocatalysts including TiO_2 [8], CdS [9], SnS_2 [10], and Ag_2S [11]. Compared with the traditional photocatalysts, the advantage of the MOFs as photocatalysts for Cr(VI) reduction results from their desirable topology and high surface and interface area, which can facilitate fast mass transport [12,13]. During the photocatalytic Cr(VI) reduction process, dissolved organic acids were often selected as hole scavenger to boost the separation efficiency of the photo-induced electrons and holes [14-17], considering that acids present widely in natural environments.

In general, powder photocatalysts including MOFs (metal–organic frameworks) particles are difficult to recover and recycle. In addition, powder MOFs suffer from the poor water stability. Recently, MOF-based free-standing membranes and thin films has been extensively studied for applications in optics [18], microelectronics [19], sensing [20], as well as energy conversion & storage [21,22]. Our group previously reported that the UiO-66-NH_2(Zr/Hf) membranes exhibited both outstanding reusability and water stability, which can achieve 94% Cr(VI) reduction efficiency after 20 cycles within 2400 min [12].

Inspired by our previous work, α-Al_2O_3 sheet prepared via solid-phase reaction [23] was adopted as the substrate to immobilize MIL-101(Fe)–NH_2 due to the excellent surface properties, electrical insulation and good strength. MIL-101(Fe)–NH_2 was selected to be immobilized onto α-Al_2O_3 substrate (MIL-101(Fe)–NH_2@Al_2O_3, MA) via reactive seeding method for photocatalytic Cr(VI) reduction in batch scale and continuous operation modes under white light. Oxalic acid was introduced as a hole trapping agent to further improve the photocatalytic Cr(VI) reduction performance of MA photocatalyst. The photocatalytic Cr(VI) removal over the MA photocatalyst is featured with the following advantages. Firstly, MA photocatalyst enables to overcome the aggregation and difficult recycling of powder MIL-101(Fe)–NH_2

* Corresponding author.
E-mail addresses: wangchongchen@bucea.edu.cn, chongchenwang@126.com (C.-C. Wang).

https://doi.org/10.1016/j.cej.2021.132497
Received 27 July 2021; Received in revised form 1 September 2021; Accepted 13 September 2021
Available online 17 September 2021

photocatalysts. Secondly, MA photocatalyst exhibits satisfied photocatalysis performance and reusability to reduce Cr(VI) upon the irradiation of white light with the aid of oxalic acid. Finally, the continuous Cr (VI) reduction operation was accomplished over MA photocatalyst in the home-made fixed bed reactor. This work provides a possibility of applying MOFs as photocatalyst for purification of wastewater containing Cr(VI) pollutant.

2. Experimental

2.1. Materials and characterization

All used chemicals, characterization instruments and methods are provided in the Supplementary Information (SI).

2.2. Preparation of MA photocatalyst

The alumina support was produced according to our previous report [12]. The MA photocatalyst was fabricated via secondary seeding growth method [24]. The synthesis procedure includes two steps. (i) Seed growth: The homogeneous matrix of 2-aminoterephthalic acid (NH_2-BDC, 1.98 mM, 0.3586 g), 25.0 mL deionized water and α-Al_2O_3 was sealed into a Teflon-lined bomb (100.0 mL) to react hydrothermally at 453 K for 12 h. Afterward, the seeded α-Al_2O_3 support was washed with water, followed by being dried at 333 K for 6 h. (ii) Secondary growth: a synthetic solution was prepared by mixing the $FeCl_3{\cdot}6H_2O$ (1.98 mM, 0.5350 g), 2-aminoterephthalic acid (NH_2-BDC, 1.98 mM, 0.3586 g), N,N-dimethylformamide (DMF, 45.0 mL) and acetic acid (1.8 mL). The mixture and the seeded α-Al_2O_3 support were sealed into a 100.0 mL Teflon-lined bomb to be heated at 383 K for 24 h. Finally, the MA photocatalyst was cleaned with DMF to remove the unreacted reactants and then dried at 333 K for 6 h.

2.3. The batch test of photocatalytic Cr(VI) reduction over MA photocatalyst

The batch-scale tests of the photocatalytic Cr(VI) reduction into Cr (III) over the MA photocatalyst were performed at room temperature in a quartz reactor as illustrated in **Fig. S1**, in which the 50.0 mL Cr(VI) aqueous solution with initial concentration of 5.0 mg/L was irradiated using a 300 W Xe lamp (Beijing Aulight Co., Ltd, and the white light spectrum was depicted in **Fig. S2**). It has been reported that the addition of organics as hole trapping agents can significantly accelerate the photocatalytic Cr(VI) reduction reaction, which can be ascribed to the boosted separation of photo-generated electron-hole pairs [25]. Therefore, 2.0 mL oxalic acid (0.8 mM) was added to the reaction solution. During the light irradiation, 1.5 mL solutions were extracted by syringe filter with 0.22 μm PTFE membrane at pre-set time intervals. The diphenylcarbazide colorimetric method over the Auto Analyzer 3 (169 + B205-01) was selected to test the concentration of the residual Cr(VI) [26].

The apparent quantum efficiency (AQE) of the MA as photocatalyst was calculated according to Eq. (1) on the basis of the amount of the reduced Cr(VI) at a given monochromatic irradiation provided by a 300 W Xe lamp with the different filters [27].

$$AQE(Cr) = \frac{3 \times [number\ of\ reduced\ Cr(VI)]}{number\ of\ incident\ photons} \quad (1)$$

2.4. The continuous operation of photocatalytic Cr(VI) reduction over MA photocatalyst

A home-made fixed bed reactor system (Scheme 1) was adopted to achieve continuous operation for photocatalytic Cr(VI) reduction over MA photocatalyst. Some related information concerning the size of reactor, area of alumina sheet was listed in **Table S1**. As illustrated in Scheme 1, the model hexavalent chromium solution (5.0 mg/L) was delivered by a peristaltic pump (Peek 6000LDI-P) at the flow rates of 0.100 L/h, in which the oxalic acid (20 mM) with the injection speed of 0.066 mL/min injected by a high precision injection pump. At the same

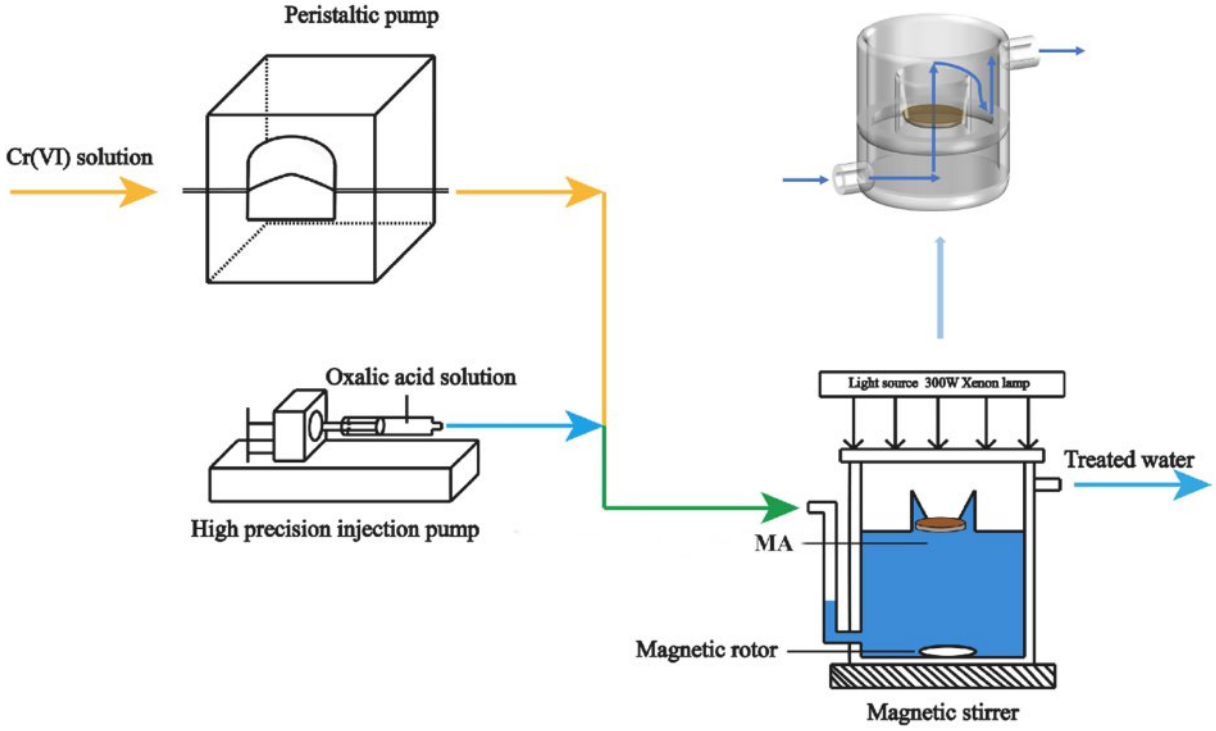

Scheme 1. Schematic overview of fixed bed reactor system for the continuous photocatalytic Cr(VI) reduction operation.

time, 300 W Xe lamp (Beijing Aulight Co., Ltd) was selected as the light source matching with the fixed bed reactor.

The continuous operations for photocatalytic Cr(VI) removal over the MA photocatalyst were accomplished under the real solar light from 7:00 AM to 7:00 PM in Daxing campus of Beijing University of Civil Engineering and Architecture to study the performance in possible practical applications.

3. Results and discussion

3.1. The characterizations of the as-prepared MA photocatalyst

The fabrication procedure of the MIL-101(Fe)–NH_2 on the α-Al_2O_3 support via the secondary seeding growth method was illustrated in Fig. 1**a**. After the first seed growth step, the surface of α-Al_2O_3 support changed from white to gray, then to deep brown after the secondary growth step. Compared with the blank α-Al_2O_3, the morphology of the seeded layer over α-Al_2O_3 support was denser than that of the pristine α-Al_2O_3 sheet (**Fig. S3**), implying NH_2-BDC was adhered onto the α-Al_2O_3 support.

Due to the small content, the as-prepared MIL-101(Fe)–NH_2 on the support can't be directly characterized by SEM and XRD. However, the SEM-EDS results revealed that Fe and N elements, two characteristics elements in MIL-101(Fe)–NH_2 (Fig. 1**d**).

Transmission electron microscopy (TEM) (Fig. 2**a and 2b**) and high-resolution transmission electron microscopy (HRTEM) images (Fig. 2**c**) indicate that the average particles sizes of uniform MIL-101(Fe)–NH_2 immobilized on α-Al_2O_3 substrate ranged from 100 to 200 nm, which were smaller than the sizes of the irregular MIL-101(Fe)–NH_2 particles (200 – 1000 nm) deposited on the bottom of the reactor (**Fig. S3c**). Especially, MIL-101(Fe)–NH_2 nanoparticles were observed to be wrapped by the α-Al_2O_3 sheet (Fig. 2**c**), which was consistent with the previous report [28]. The TEM-EDS elemental mappings (Fig. 2**d**) further confirmed that the characteristic elements like Fe, N, Al, and O were evenly distributed over the as-prepared sample. Taken together, the SEM, TEM and HRTEM analysis confirmed that the successful loading of the MIL-101(Fe)–NH_2 on the α-Al_2O_3 support.

The surface morphologies of the pristine α-Al_2O_3 support and MA photocatalyst was observed by atomic force microscope (AFM), which provided more evidence for the successful decoration of MIL-101(Fe)–NH_2 onto α-Al_2O_3 support. The 2D AFM images and corresponding 3D AFM images were showed in Fig. 3. The roughness parameters of the MA photocatalyst were estimated with the AFM scanning area of 4 μm × 4 μm and 5 μm × 5 μm. It could be observed that the Rq (Rms roughness) value of MA photocatalyst was ca. 186 nm, which was obviously higher than that of the pure α-Al_2O_3 support.

The XPS characterization was performed to further detect the surface compositions of a membrane [29]. It can be observed (Fig. 4**a**) that the two peaks at 711.3 eV and 724.30 eV were ascribed to Fe $2p^{3/2}$ and Fe $2p^{1/2}$ of Fe (III) in MIL-101(Fe)–NH_2, respectively [30], which can be further affirmed by the presence of the satellite peak at 716.4 eV [31] and 728.7 eV [32]. However, the interior chemical compositions of the

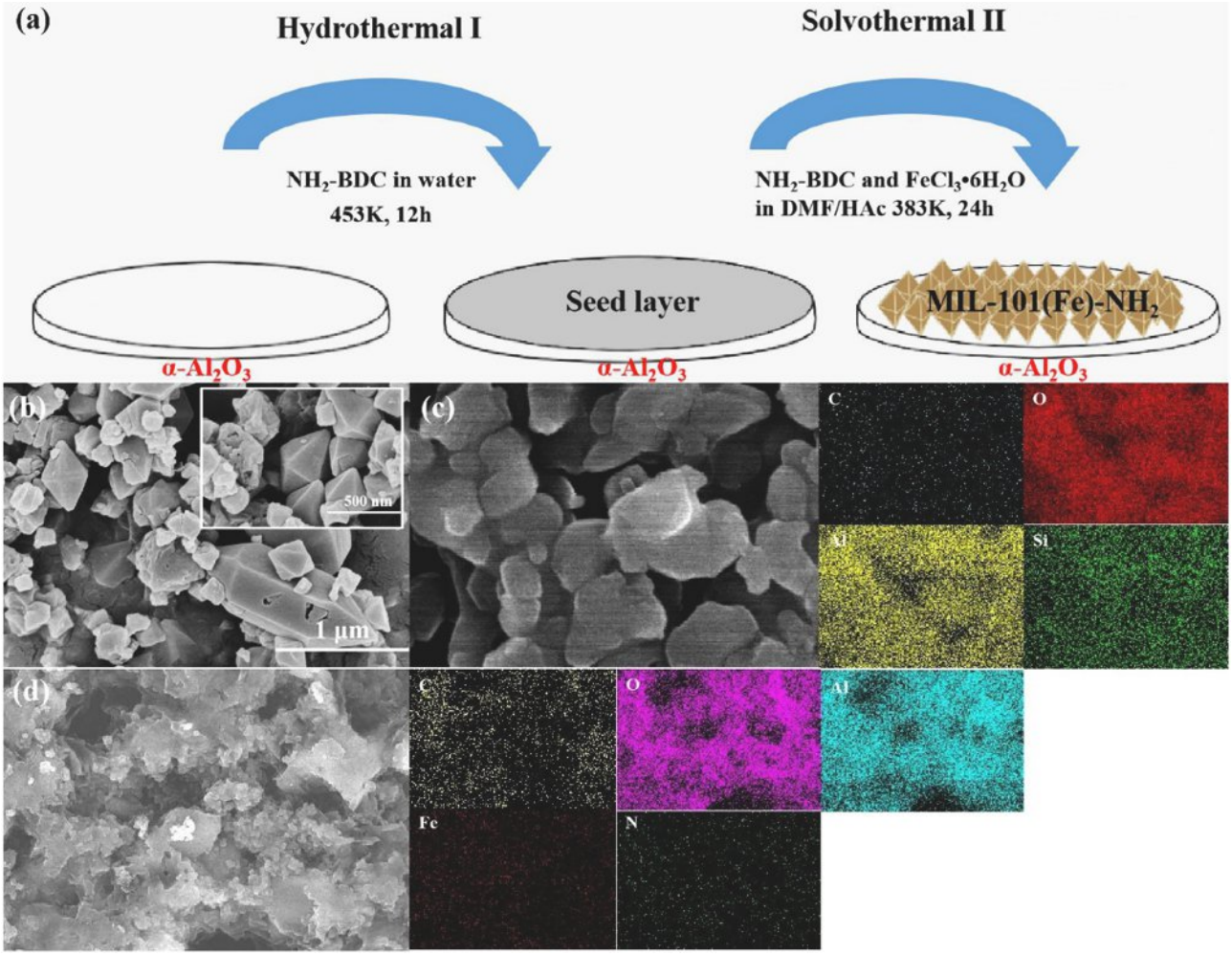

Fig. 1. (a) MA photocatalyst preparation procedure. SEM images of the (b) Bottle bottom sediment- MIL-101(Fe)–NH_2. The EDS elemental mappings of (c) α-Al_2O_3 support and (d) MA photocatalyst.

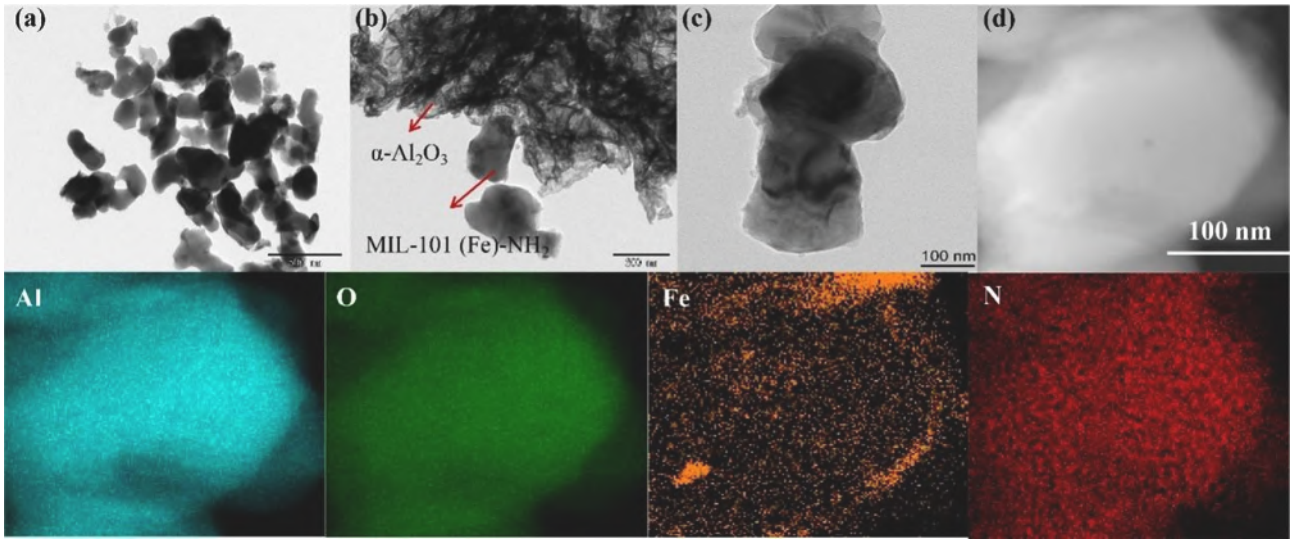

Fig. 2. TEM images of (a) MIL-101(Fe)–NH_2 from MA powder, (b) MIL-101(Fe)–NH_2 and α-Al_2O_3 powder scraped off the as-prepared MA, (c) HRTEM image of MIL-101(Fe)–NH_2 immobilized on α-Al_2O_3, (d) HRTEM-EDS elemental mappings of MA photocatalyst.

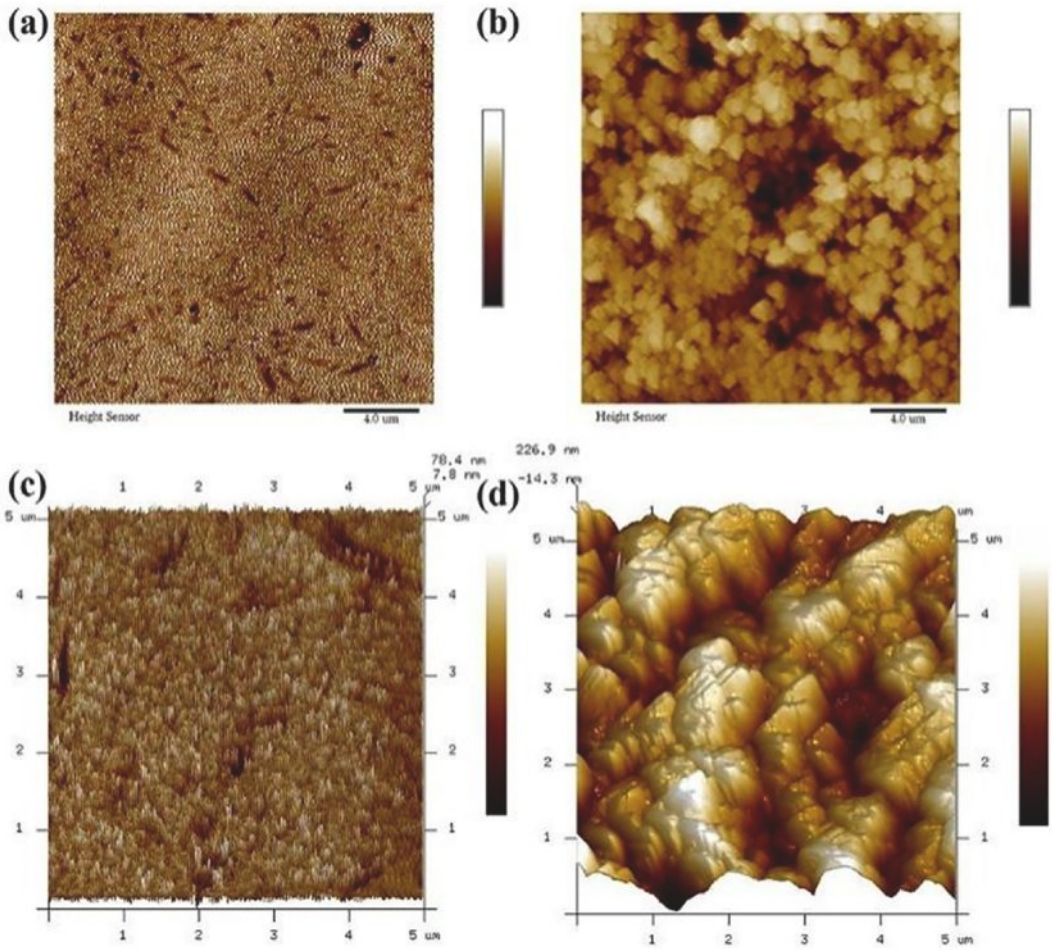

Fig. 3. 2D AFM images and corresponding 3D AFM images of the (a) and (c) α-Al_2O_3 support, (b) and (d) MA photocatalyst surface.

MIL-101(Fe)–NH_2@Al_2O_3 (MA) can't be directly detected by XPS, due to that the maximum effective determination depth of XPS was<10 nm [33]. In this study, XPS combined with argon beam etching technique was adopted to investigate the elemental distribution at different depths of MIL-101(Fe)–NH_2@Al_2O_3 (MA). The thickness of formed MIL-101 (Fe)–NH_2 was determined using an etching rate of 0.25 nm/s. After 4 runs' etching, in which each etching period was 20 s, the thickness of the MIL-101(Fe)–NH_2 loaded on the alumina substrate can be calculated as ca. 20 nm. After each etching, the distribution of elements of Fe, C, Al in each layer was nearly identical, indicating that a uniform MIL-101(Fe)–

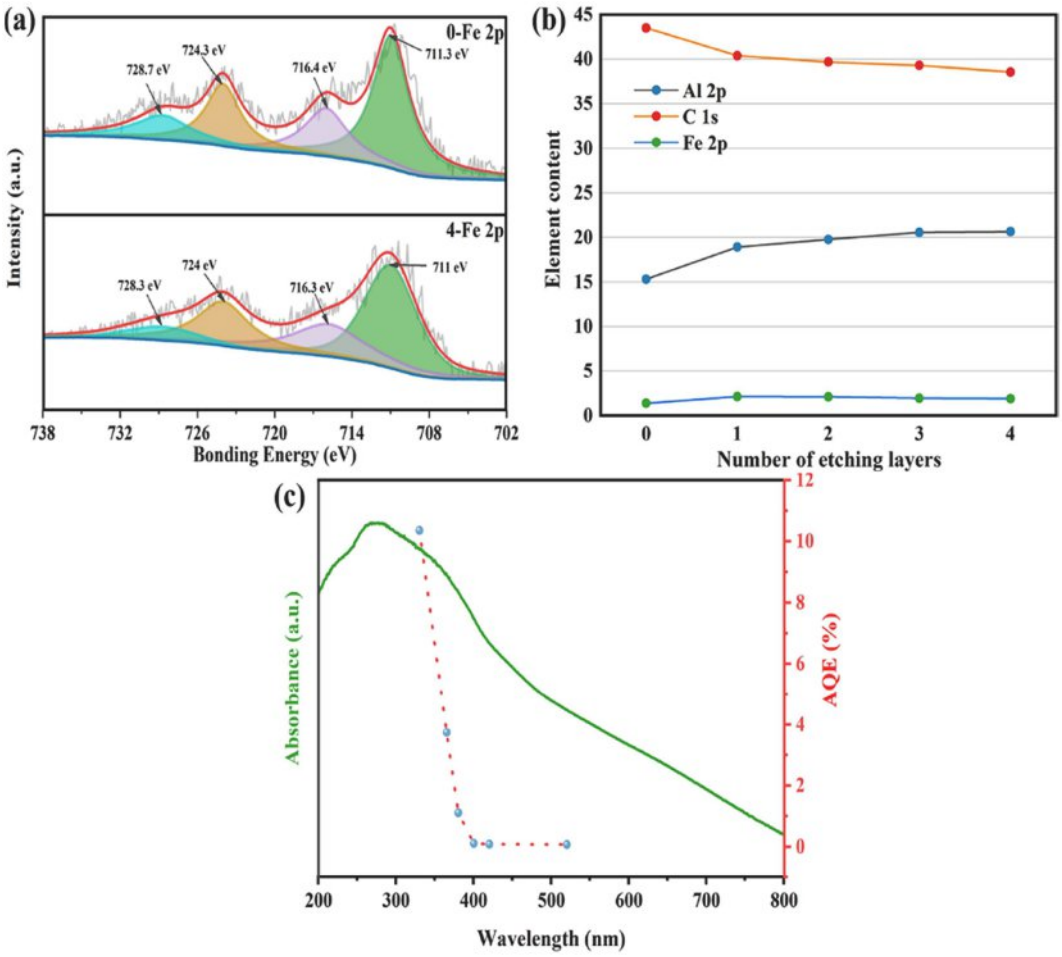

Fig. 4. (a) XPS spectra of MIL-101(Fe)–NH_2@Al_2O_3 (MA). (b) Elements (Al, C, Fe) contents in different etching layers of the as-prepared MIL-101(Fe)–NH_2@Al_2O_3 (MA). (c) AQE of Cr(VI) reduction upon the irradiation of white light. Reaction conditions: the actual MIL-101(Fe)–NH_2 was ca. 15.0 mg per sheet, 50 mL of 5 mg/L Cr(VI), oxalic acid = 0.8 mM, initial solution pH = 3.4.

NH_2 was immobilized onto the α-Al_2O_3 substrate. As shown in Fig. 4**b**, from the surface to the fourth layer of etching, there was a minor increase of iron content, in which the presence of surface pollution from deposited carbon may lead to the decreasing iron content [34].

The optical absorption activity of the MA photocatalyst was investigated by UV–vis diffuse reflection spectra (UV–vis DRS). As illustrated in **Fig. S4**, both MIL-101(Fe)–NH_2 powder and MA photocatalyst displayed the superior light absorption in the range of 200 – 800 nm, which resulted from both the Fe-O clusters and –NH_2 group of BDC linker in MIL-101(Fe)–NH_2 [35,36]. The apparent quantum efficiency (AQE) at different wavelengths was deemed as a key index of evaluating photocatalytic activity under different light [37]. As illustrated in Fig. 4**c**, the Cr(VI) reduction AQEs over MIL-101(Fe)–NH_2@Al_2O_3 (MA) were 10.35%, 3.73%, 1.10%, 0.10%, 0.09% and 0.07% at the light

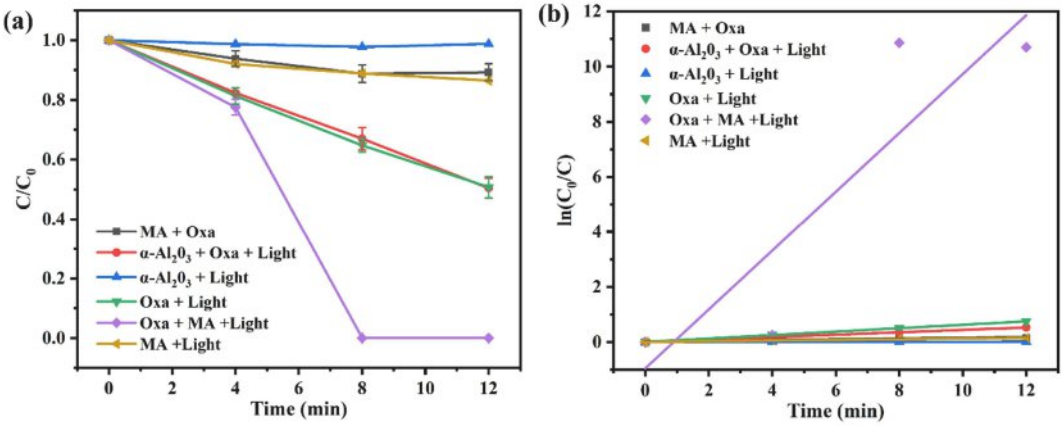

Fig. 5. (a) The photocatalytic Cr(VI) reduction and (b) the rates (*k* values) over the samples over white light irradiation under different systems. Reaction conditions: the actual MIL-101(Fe)–NH_2 was ca. 15.0 mg per sheet, 50 mL of 5 mg/L Cr(VI), oxalic acid = 0.8 mM, initial solution pH = 3.4.

wavelength of 330 nm, 365 nm, 380 nm 400 nm 420 nm and 520 nm, respectively, which fitted perfectly with the plot of UV–vis DRS spectra of the MIL-101(Fe)–NH_2@Al_2O_3. These AQEs results further affirmed that Cr(VI) reduction was a photo-induced reaction [37,38].

3.2. Photocatalytic Cr(VI) reduction performance of MA photocatalyst

The photocatalytic Cr(VI) reduction performance of MA photocatalyst was evaluated with oxalic acid as both reductant and hole capture agent. Under the irradiation of white light, only ca. 14.0% Cr (VI) can be removed in the presence of MA photocatalyst (Fig. 5**a**), indicating that effective Cr(VI) reduction can't be achieved via photocatalysis process over MA photocatalyst without the aid of oxalic acid. Only oxalic acid under white light irradiation can achieve nearly 35.2% Cr(VI) removal with the absence MA photocatalyst as catalyst within 8.0 min, indicating that Cr(VI) can be photo-reduced by oxalic acid as reductant [39,40]. However, with the presence of both white light and oxalic acid, the 100% Cr(VI) with initial concentration of 5 mg/L can be removed by MA photocatalyst within 8.0 min. The photocatalytic reduction of Cr(VI) approximately follows pseudo-first-order kinetics, the corresponding reduction rate constant K_{obs} over MA photocatalyst as photocatalyst with the presence of oxalic acid was 1.068 min^{-1}, which was ca. 84.88, 24.54 and 970.74, 17.17, 92.05 times faster than those of the MA/Oxa, α-Al_2O_3/Oxa/light, α-Al_2O_3/light, Oxa/light, MA/light system. Therefore, the effective Cr(VI) removal was contributed the synergic effect of photocatalytic reduction and light-induced oxalic acid reduction over MA photocatalyst, in which oxalic acid can act as not only reductant to directly reduce Cr(VI) but also hole capture agent to promote the separation and migration of electron-holes.

Generally, the pH of the treated water sample can affect the adsorption and photocatalysis processes, since it could influence on both the species of Cr(VI) ions and the surface charge of the photocatalyst [41]. As shown in Fig. 6**a and 6b**, the photocatalytic Cr(VI) reduction performances, such as efficiencies and rates (*k* values) of the MA photocatalyst, varied obviously with pH. Specifically, the Cr(VI) photoreduction efficiencies increased rapidly with the decreasing pH values (97.8%, 97.7%, 97.6%, 96.4%, 51.6% at pH = 2, 4, 6, 8 and 10, respectively). Under acidic environments, the Cr(VI) photoreduction over MA photocatalyst was achieved following Eq. (2), (3) and (4) [8,13]. With 2 < pH < 6, the dominate Cr(VI) species were $Cr_2O_7^{2-}$ or $HCrO_4^-$. In addition, the Cr(VI) was easily reduced by oxalic acid in acidic medium following Eq. (5). Under alkaline environment, CrO_4^{2-} was the main existence form and the corresponding Cr(VI) reduction was accomplished following Eq. (6) [42]. Obviously, acidic medium favored the Cr(VI) photoreduction due to the amount of substantial H^+.

MA photocatalyst + $h\nu$ → MA photocatalyst ($h^+ + e^-$) (2)

$Cr_2O_7^{2-} + 14H^+ + 6e^- \rightarrow 2Cr^{3+} + 7H_2O$ (3)

$HCrO_4^- + 7H^+ + 3e^- \rightarrow Cr^{3+} + 4H_2O$ (4)

$Cr_2O_7^{2-} + 3HC_2O_4^- + 11H^+ \rightarrow 2Cr^{3+} + 6CO_2 + 7H_2O$ (5)

$CrO_4^{2-} + 4H_2O + 3e^- \rightarrow Cr(OH)_3 + 5OH^-$ (6)

When pH greater than 6, increasing $Cr(OH)_3$ precipitates can be deposited on the surface of photocatalyst to mask its active sites, which led to the decreased photocatalytic Cr(VI) reduction performance [43]. However, after adding oxalic acid as both reductant and the hole trapping agent, the alkaline solution was adjusted to an acidic solution, which can explain why the MA has a good performance in reducing Cr (VI) in a wide initial pH range.

The isoelectric point of MIL-101(Fe)–NH_2 was measured to be

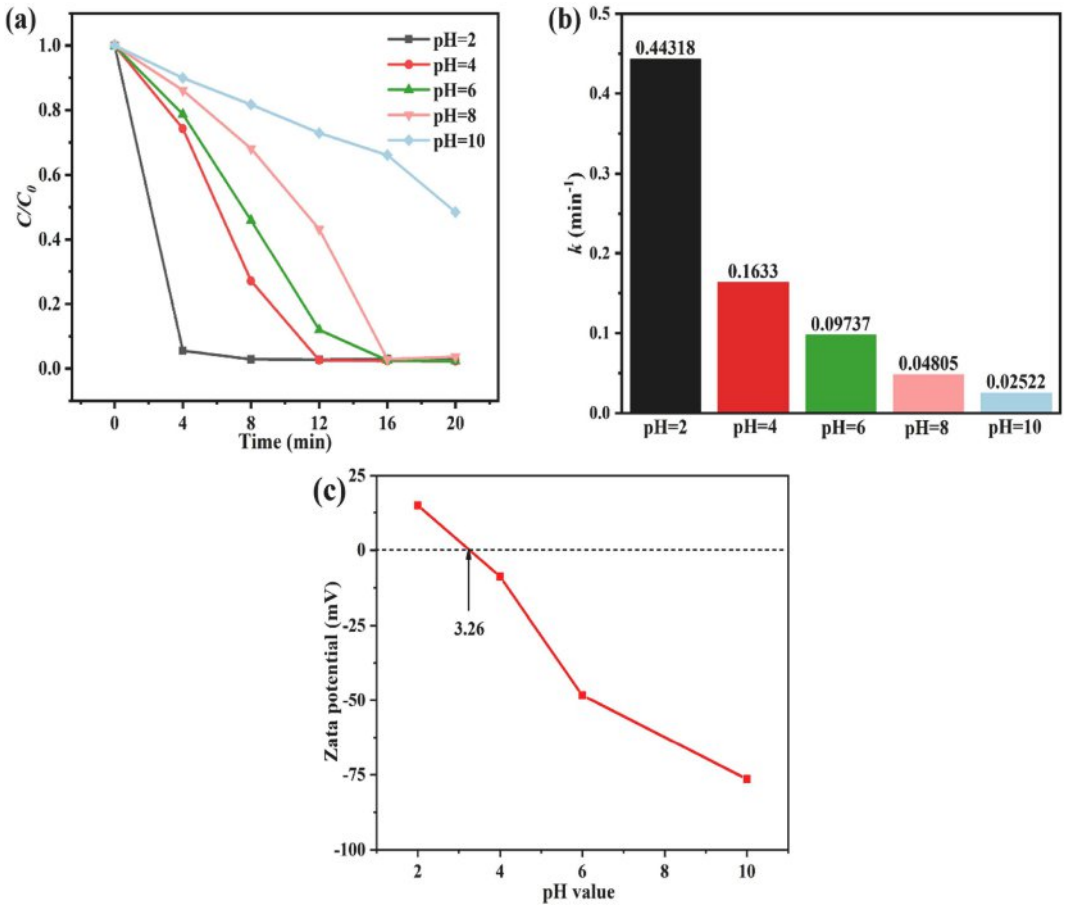

Fig. 6. (a) Influence of pHs on Cr(VI) reduction efficiencies. Reaction conditions: the actual MIL-101(Fe)–NH_2 was ca. 15.0 mg per sheet, 50 mL of 5 mg/L Cr(VI), oxalic acid = 0.8 mM (b) The *k* values over the different pHs. (c) The surface zeta potential versus pH of MIL-101(Fe)–NH_2.

ca.3.26, indicating that the zeta potential of the MIL-101(Fe)–NH_2 was positive when the pH < 3.26. Hence, the positive surface of MIL-101 (Fe)–NH_2 under acid conditions was inclined to adsorb anionic Cr(VI) due to the electrostatic attraction, which can favor the capture of photo-generated electrons to accomplish superior Cr(VI) photoreduction efficiency [2]. Considering the stability of the MIL-101(Fe)–NH_2 in an acidic environment [44], we chose the initial pH (3–5) of the Cr(VI) solution as an optimal condition.

Besides solution pH, the dosage of oxalic acid also played an important role in the Cr(VI) reduction [40]. Therefore, a new series photoreduction experiments were performed, in which different Cr(VI) (5 mg/L): oxalic acid molar ratios (2:1, 4:1, 6:1, 8:1 and 10:1) were selected to explore the influence of oxalic acid concentrations. As shown in **Fig. S5a**, Cr(VI) reduction efficiencies increased with the increase of oxalic acid dosage. Obviously, the Cr(VI) reduction efficiency did not improved significantly when the n(Oxa)/n(Cr) molar ratios increased from 4:1 to 10: 1. In order to achieve a better treatment of industrial wastewater, we chose the n(Oxa)/n(Cr) = 8.4:1 (0.8 mM oxalic acid) as an optimal condition in further experiments. The effect of Cr(VI) concentration on the reduction efficiency of Cr(VI) was investigated by various initial concentration from 5 to 30 mg/L (**Fig. S5b**). The reduction efficiency of Cr(VI) decreased with the increasing of Cr(VI) concentration, which may be caused by excessive chromate occupying the active sites of MA photocatalyst, which was similar to the previous literature [45,46].

Both the co-existing inorganic ions and the dissolved organic matters (DOM) might impact the Cr(VI) photoreduction efficiencies, which were investigated by the Box-Behnken statistical experimental design approach. Generally, many inorganic cations like Na^+, K^+ and Ca^{2+} with stable and highest oxidation states demonstrated insignificant effect on the Cr(VI) reduction process, due to that they were inert to the photo-induced electrons or holes [47]. As listed in **Table S2**, a total of 17 experiments taking the account of three factors like oxalic acid (A), SO_4^{2-} (B) and Cl^- (C) were designed to determine the optimum Cr(VI) reduction conditions under white light. The designed experiments (17 runs) were depicted in **Table S3**, in which the response (photocatalytic efficiency %) and variables can be expressed as Eq. (7).

$$\text{Efficiency \%} = 34.44 + 3.90A - 6.95B - 3.80C + 1.87AB + 5.93AC - 1.17BC + 34.14A^2 + 28.05B^2 + 23.99C^2 \quad (7)$$

As shown in **Table S4**, the analysis of variance ANOVA was applied to test the availability of Box-Behnken design for Cr(VI) removal. It can be observed from the ANOVA results of photocatalytic Cr(VI) efficiencies that the determination coefficient displayed a high value (R^2 = 0.98), indicating that 98.0 % of the variability in the response could be predicted by the model. The P-values were used to check the significance of each coefficient and to verify the interaction strength of each parameter. Values of Prob F were < 0.0001, implying that the model was statistically significant. In addition, it can be concluded from the F value **(Table S4)** of the variable that the influence order of the three variables on the reduction of Cr(VI) was B (SO_4^{2-}) > A (oxalic acid) > C (Cl^-). It can be seen that as the concentration of inorganic anions increases constantly, the Cr(VI) photoreduction efficiencies decreases initially, followed by an obvious increase (Fig. 7). It was found that SO_4^{2-} ions exerted negative impact on the photocatalytic Cr(VI) reduction, because SO_4^{2-} ions can be competitively adsorbed onto MA photocatalyst resulting from the electronic interactions [13]. The highest Cr(VI) reduction efficiency can be accomplished under the optimal concentrations of oxalic acid, SO_4^{2-} and Cl^- being 162.05, 10757, and 31103 mg/L, respectively.

3.3. Reusability of MA photocatalyst

As in Fig. 8**a**, the Cr(VI) reduction efficiencies over MA photocatalyst upon the irradiation of white light can be maintained at 100.0% for at least 20 runs (totally 400 min). By calculating the peak area of N 1 s of MA before and after Cr(VI) reduction (**Fig. S6**), it was found that MA still maintained its composition after 20 runs' operations of Cr(VI) reduction experiments, indicating its good stability and reusability. The XPS spectra (Fig. 8**d**) of used MA matched well with fresh samples, which could further confirm its stability. Furthermore, the concentrations of leached Fe in the acidic condition were determined by ICP-OES as 0.75 mg/L, which met the requirement of the environmental standards (2 mg/L) set by the European Union. It can be concluded that MA with the assistance of oxalic acid exhibited outstanding photocatalytic performances and reusability, which can exceed most counterparts (**Table S5**).

3.4. The continuous operation of photocatalytic Cr(VI) reduction over MA photocatalyst in a fixed-bed reactor

To utilize the high reusability of the MA, a micro fixed bed reactor (Scheme 1) was designed and fabricated to accomplish the continuous operation of photocatalytic Cr(VI) reduction. The residence time (T) of the treated solution was calculated by the approach proposed by Martínez et al.[48]. For the operating conditions used in this work, the hydraulic retention time (HRT) was calculated to be 120 min. For the purpose of maintaining the ratio of different solutions in batch experiment and fixed bed reactor, the flow rate of Cr(VI) solution and oxalic acid solution was calculated based on the Eq. (8). Therefore, the flow rate of Cr(VI) solution and oxalic acid solution was set at 0.100 L/h and 0.066 mL/min, respectively.

$$Q_{Cr(VI)}/Q_{Ox} = V_{Cr(VI)}/V_{Ox} \quad (8)$$

Where, $Q_{Cr(VI)}$ and Q_{Ox}: the flow rate of Cr(VI) solution (L/h) and oxalic acid (mL/min); $V_{Cr(VI)}$ and V_{Ox}: liquid volume of Cr(VI) solution and oxalic acid (mL); V: the effective volume of the fixed bed reactor (mL).

As illustrated in Fig. 8**b**, nearly 100% Cr(VI) with initial concentration of 5 mg/L can be photo-catalytically removed up to 30 h. From 30 – 45 h, more than 90% Cr(VI) can be reduced in this continuous operation

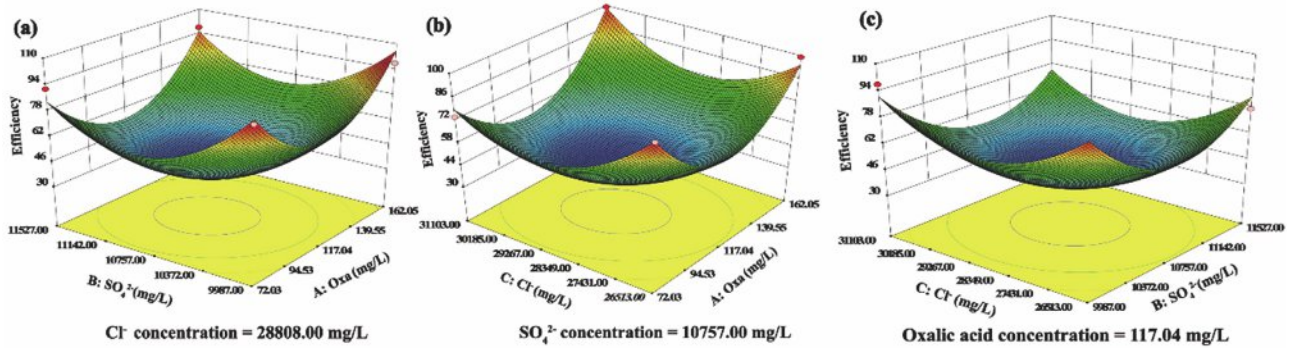

Fig. 7. (a)~(c) Response surface plots of Cr(VI) reduction efficiencies versus the influences of the three variables. Reaction conditions: the actual MIL-101(Fe)–NH_2 was ca. 15.0 mg per sheet, 50 mL simulated wastewater containing Cr(VI) with initial concentration of 10 mg/L, initial solution pH = 3.35.

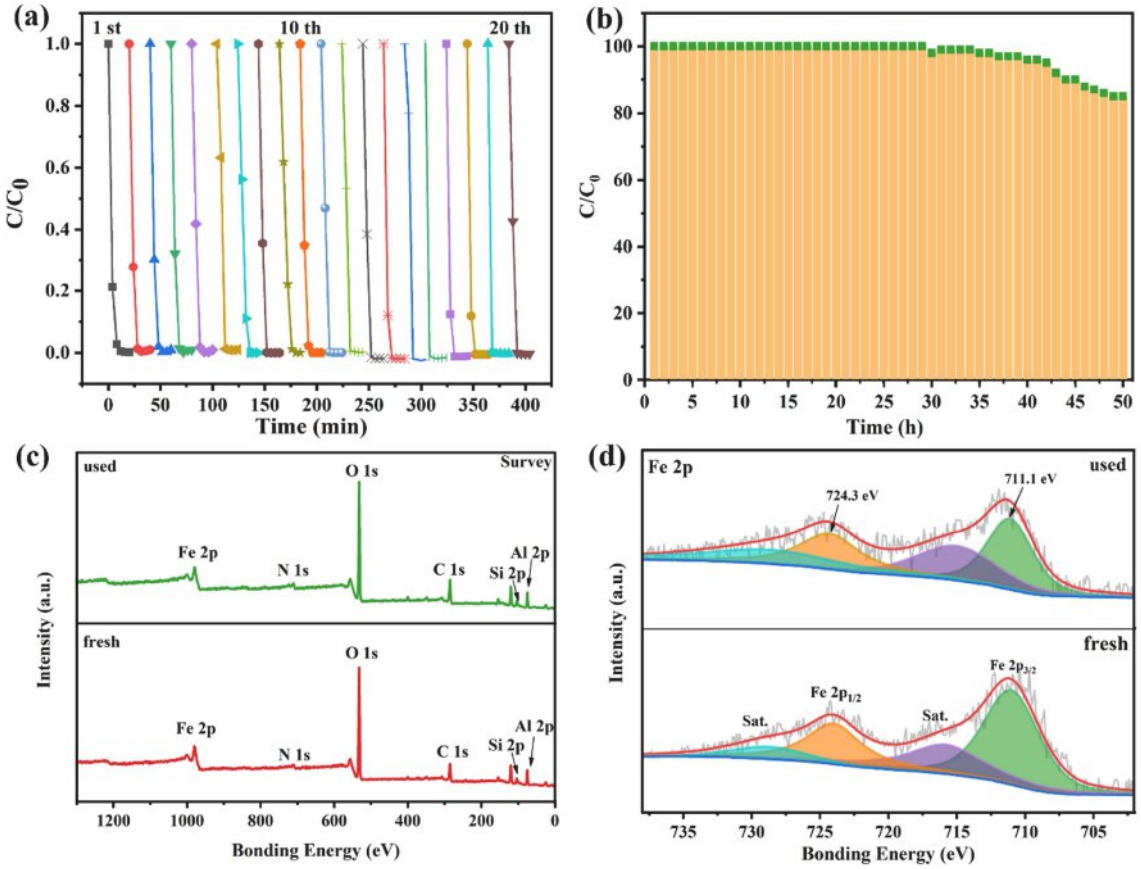

Fig. 8. (a) Batch-scale reusability test of Cr(VI) reduction over MA under white light irradiation. (b) Continuous operation Cr(VI) reduction performance of MA in fixed bed reactor. (c) XPS survey scan and (d) Fe 2p spectra of MA after Cr(VI) reduction. Reaction conditions: the actual MIL-101(Fe)–NH_2 was ca. 15.0 mg per sheet, Cr(VI) = 5 mg/L, oxalic acid = 0.8 mM, 300 W white light irradiation, initial solution pH = 3.4.

system. Finally, from 45 h to 50 h, the Cr(VI) reduction efficiency decreased to ca. 80%. Considering that the average load of MIL-101(Fe)–NH_2 over a piece of α-Al_2O_3 was 15 mg and the device's flow rate as well as operation period were 0.100 L/h and 50 h, it can be calculated that one kilogram of MIL-101(Fe)–NH_2 can treat as much as 33.3 T wastewater containing 5 mg/L Cr(VI).

3.5. The mechanism of photocatalytic Cr(VI) reduction

The trapping experiments were performed to explore the Cr(VI) reduction mechanism over MA photocatalyst, in which benzoquinone (BQ) [49], isopropyl alcohol (IPA) [13] and $KBrO_3$ with concentrations of 0.2 mM were selected to capture $\bullet O_2^-$, •OH and e^-, respectively (Fig. 9**a**). According to previous reports, $\bullet O_2^-$ was generated from the reaction between the dissolved oxygen and the photo-generated electrons over the photocatalysts under light illumination, which can also react with Cr(VI) to generate Cr(V) and Cr(III) during photoreaction process [50,51]. It was reported that •OH formed from the oxidation of H_2O or OH^- by holes could favor the separation of electrons and holes to accomplish the boosted Cr(VI) reduction activity [51]. However, in this study, a minor decrease of Cr(VI) reduction efficiency can be found after the addition of BQ and IPA, implying that $\bullet O_2^-$ and •OH exerted slight effect to the Cr(VI) reduction. About 54.9% suppression can be observed (Fig. 9**a**) as the photo-induced electrons were captured by the adding $KBrO_3$, indicating that the photo-generated electrons played the dominating role of for Cr(VI) reduction. The trapping experiment results indicated that the photo-induced electrons rather than $\bullet O_2^-$ was the primary active specie to reduce Cr(VI), which was quite different with our previous observation [13].

ESR analyses were applied to verify the existence radicals to further explore the effect of oxalic acid on the Cr(VI) photoreduction. As shown in Fig. 9**b**, no noticeable ESR peaks were observed in blank experiment. When the MA photocatalyst was added without light, only the DMPO-•OH adducts were detected as a four-line (1:2:2:1) ESR signals with g = 2.0055 [52]. Once upon the irradiation of white light, the signals of DMPO-•OH spin disappeared completely; while the six-line ESR signals with g = 2.0036 corresponding to the DMPO-$CO_2^{\bullet-}$ adducts were detected [53], indicating that the formed $CO_2^{\bullet-}$ radicals can be responsible to the Cr(VI) reduction. It was proposed that there were two ways to boost the Cr(VI) reduction. (1) Upon the irradiation of white light, the MA photocatalyst was excited to yield holes and electrons (Eq. 9), in which the oxalic acid adsorbed on the surface of photocatalyst would be oxidized by the holes to form $CO_2^{\bullet-}$ radicals (Eq. 10) [54] for promoting the Cr(VI) reduction (Eq. 11). At the same time, the effective separation of holes and electrons can further enhance the Cr(VI) reduction via the consumption of electrons (Eq. 12). (2) The oxalic acid itself could produce $CO_2^{\bullet-}$ radicals under white irradiation to reduce Cr(VI) into Cr(III) [55].

MA photocatalyst → $e^- + h^+$ (9)

$h^+ + HC_2O_4^- \rightarrow CO_2^{\bullet-} + CO_2 + H^+$ (10)

$CO_2^{\bullet-} + Cr(VI) + H^+ \longrightarrow Cr(III) + CO_2 + H_2O$ (11)

$e^- + Cr(VI) \longrightarrow Cr(III)$ (12)

Generally, hydroxyl radical (•OH) can be detected by the fluorescence method using terephthalic acid as a probe molecule [56]. It can be observed from Fig. 9**c** that the fluorescence intensity at 425 nm decreased significantly after the addition of oxalic acid, indicating that the oxalic acid might restrain the formation of •OH radicals by directly oxidizing the photo-induced holes. This observation matched well with the above-mentioned ESR determination, in which the •OH radicals were inclined to interact with oxalic acid rather than the DMPO upon

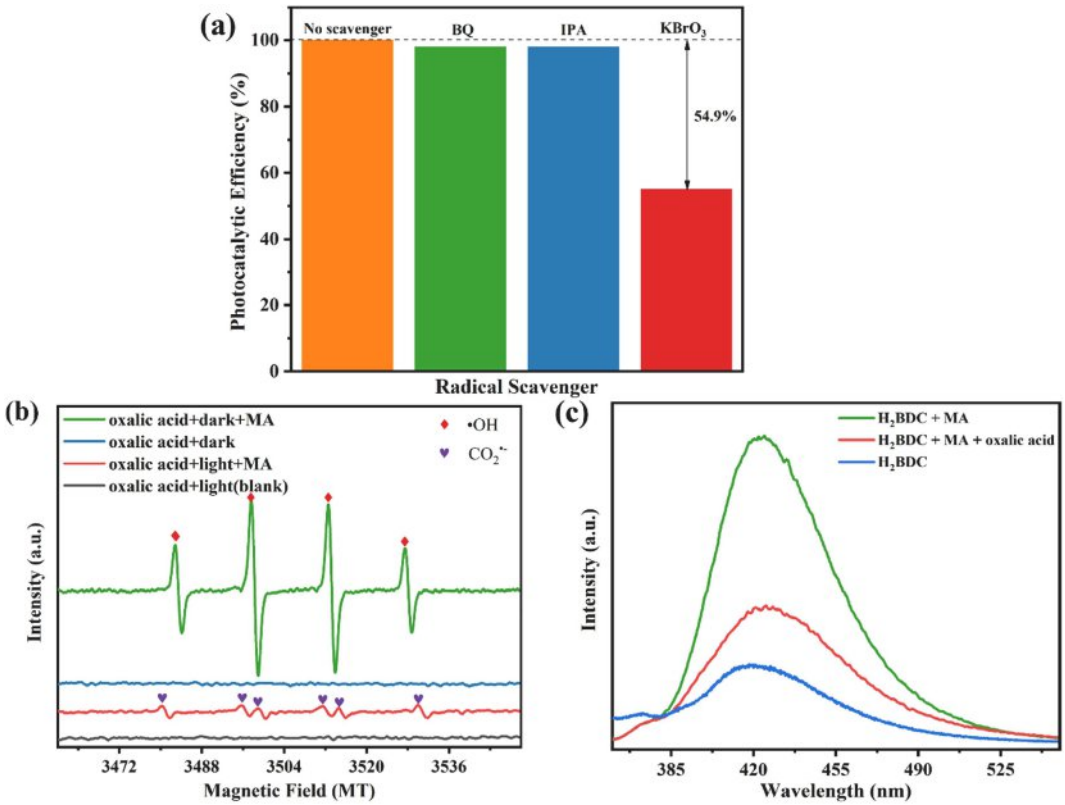

Fig. 9. (a) Reactive species trapping experiments with MA photocatalyst under white light irradiation (b) ESR spectra of the DMPO-•OH and $CO_2^{\bullet-}$ radicals for MA photocatalyst after 5 min of white light irradiation. (c) The alterations of the fluorescence intensity with and without oxalic acid.

light irradiation [57].

Based on the above experimental results, the possible Cr(VI) reduction mechanism were proposed as illustrated in Fig. 10. Under white light irradiation, in addition to the direct light absorption of the Fe − O cluster, the NH_2 group in the organic linker can both absorb visible light and transfer the electrons from the organic linkers to the Fe_3-μ_3-oxo clusters to participate the Cr(VI) reduction. The –NH_2 group in the MIL-101(Fe)–NH_2 can boost the electron transfer and electron–hole pairs separation, resulting in the enhanced photocatalytic Cr(VI) reduction performance [36]. Meanwhile, the oxalic acid plays two important roles in the reduction of Cr(VI): (1) to react with h^+ to generate $CO_2^{\bullet-}$ radicals for Cr(VI) reduction [58] and (2) to yielded $CO_2^{\bullet-}$ radicals under white irradiation to reduce Cr(VI), in which the $CO_2^{\bullet-}$ radicals effectively reacted with Cr(VI) to yield Cr(III) [59].

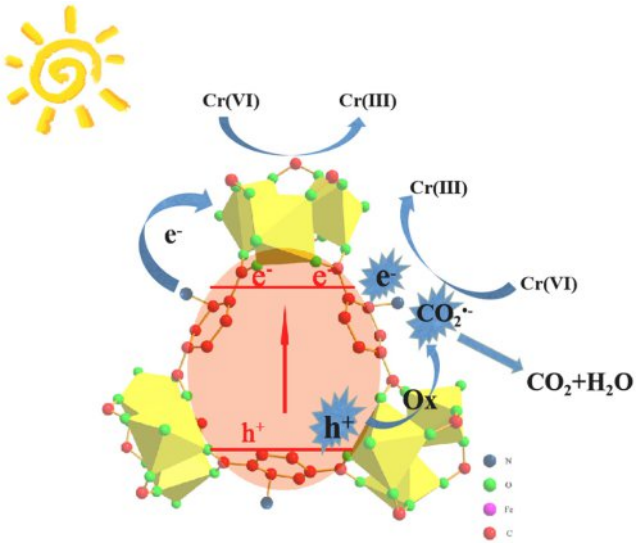

Fig. 10. Schematic illustration of the photocatalytic Cr(VI) reduction over MA photocatalyst in the presence of oxalic acid.

3.6. *Photocatalytic Cr(VI) reduction over MA photocatalyst upon the irradiation of real solar light*

3.6.1. *Batch experiment*

In this study, the photocatalytic Cr(VI) reduction over MA photocatalyst upon the irradiation of real solar light were conducted at Daxing campus of BUCEA (39°44′ N, 116°17′E) on December 11th (15 °C), 2020. The average optical power of real solar light was 55 mW. As shown in Fig. 11**a**, ca. 98.2% Cr(VI) was reduced into Cr(III) with the presence of oxalic acid within 20 min, implying that MA photocatalyst can achieve efficient photocatalysis activity under the real sunlight.

3.6.2. *Continuous operation*

The continuous operation of photocatalytic Cr(VI) reduction over MA photocatalyst in a fixed-bed reactor were conducted under real sunlight at Daxing campus of BUCEA (39°44′ N, 116°17′E) on April 28th, 2021. It can be found that MA photocatalyst can accomplish effective Cr(VI) reduction with the help of the oxalic acid under the real solar light, in which the Cr(VI) reduction activity over the photocatalyst was influenced by the solar power and the temperature from 8:00 to 18:00. As shown in Fig. 11**b**, the Cr(VI) removal efficiencies increased with the increasing solar power and temperature. It was worth noting that the enhancement of photocatalytic reduction of Cr(VI) was in proportion to actual sunlight intensity, indicating that the illumination intensity was one of the important factors to influence the Cr(VI) photoreduction. Additionally, MA photocatalyst exhibited highest efficiencies (100%) under real solar light as the optical power reached 280.3 mW at 12:00. It can be believed that the as-prepared MA

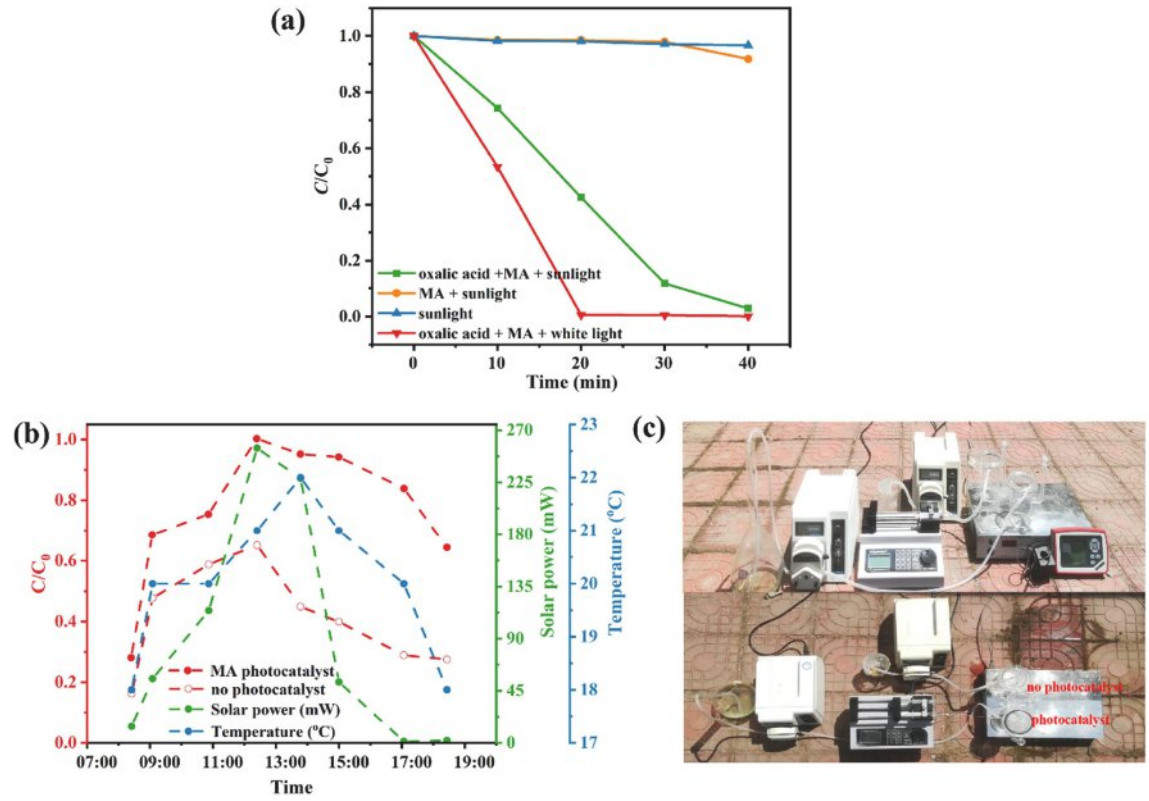

Fig. 11. (a) Photocatalytic Cr(VI) reduction under real sunlight; (b) The influence of solar power and temperature on the photocatalytic Cr(VI) reduction efficiency in the continuous fixed-bed reactor; (c) The front view and vertical view of micro membrane reaction bed device. Reaction conditions: the actual MIL-101(Fe)–NH_2 was ca. 15.0 mg per sheet, Cr(VI): 5 mg/L, 0.100 L/h, oxalic acid: batch experiment 0.8 mM, continuous operation 20 mM, 0.066 mL/min, initial solution pH = 3.3.

photocatalyst can be potentially adopted to accomplish large-scale Cr (VI) reduction with the aid of oxalic acid.

4. Conclusion

In this work, a continuous operation system based on MA photocatalyst was developed for the rapid reduction of Cr(VI). The MA photocatalyst was successfully fabricated on α-Al_2O_3 substrates by a facile reactive seeding method. The MA photocatalysts can be used in fixed-bed reactor because of their easy recovery and recyclable characteristics. It was found that one kilogram of MIL-101(Fe)–NH_2 can treat as much as 33.3 T wastewater containing 5 mg/L Cr(VI) with the synergistic effect of oxalic acid upon the white light. The Box-Behnken experiment was used to further indicate that co-existing ions and dissolved organic matter (DOM) could lead to significant impact on Cr(VI) reduction performance, which was promising for the application of Cr (VI) removal in tanning wastewater. The boosted photocatalytic performance of MA photocatalysts was attributed to e^- and $CO_2^{\bullet-}$. These findings provided a promising approach for designing the continuous membrane reaction bed based on MOFs membranes with outstanding photocatalytic Cr(VI) reduction and removal activity.

Declaration of Competing Interest

The authors declare that they have no known competing financial interests or personal relationships that could have appeared to influence the work reported in this paper.

Acknowledgements

This work was supported by National Natural Science Foundation of China (22176012, 51878023, 22176012, 21806008), Beijing Natural Science Foundation (8202016), Great Wall Scholars Training Program Project of Beijing Municipality Universities (CIT&TCD20180323), Beijing Talent Project (2020A27), Science and Technology General Project of Beijing Municipal Education Commission (KM202110016010) and The Fundamental Research Funds for Beijing University of Civil Engineering and Architecture (X20147/X20141/X20135/X20146).

Appendix A. Supplementary data

Supplementary data to this article can be found online at https://doi.org/10.1016/j.cej.2021.132497.

References

[1] G. Chen, J. Han, Y. Mu, H. Yu, L. Qin, Two-stage chromium isotope fractionation during microbial Cr(VI) reduction, Water Res. 148 (2019) 10–18.
[2] C.-C. Wang, X.-D. Du, J. Li, X.-X. Guo, P. Wang, J. Zhang, Photocatalytic Cr(VI) reduction in metal-organic frameworks: A mini-review, Appl. Catal. B 193 (2016) 198–216.
[3] M.A.G. Juan, J. Testa, M.I. Litter, Heterogeneous Photocatalytic Reduction of Chromium(VI) over TiO_2 Particles in the Presence of Oxalate: Involvement of Cr(V) Species, Environ. Sci. Technol. 38 (2004) 1589–1594.
[4] D. Petruzzelli, R. Passino, G. Tiravanti, Ind., Ion Exchange Process for Chromium Removal and Recovery from Tannery Wastes, Ind. Eng. Chem. Res. 34 (8) (1995) 2612–2617.
[5] T.J.O.S.E. Bailey, R.M. Bricka, D.D. Adrian, A review of potentially low-cost sorbents for heavy metals, Water Res. 33 (1999) 2469–2479.
[6] P. Lakshmipathiraj, G. Bhaskar Raju, M. Raviatul Basariya, S. Parvathy, S. Prabhakar, Removal of Cr (VI) by electrochemical reduction, Sep. Purif. Technol. 60 (2008) 96–102.
[7] D.L.A. Hafiane, M. Dhahbi, Removal of hexavalent chromium by nanofiltration, Desalination 130 (2000) 305–312.
[8] Y. Ku, I.-L. Jung, Photocatalytic reduction of Cr(VI) in aqueous solutions by UV irradiation with the presence of titanium dioxide, Water Res. 35 (1) (2001) 135–142.
[9] X. Liu, L. Pan, T. Lv, G. Zhu, Z. Sun, C. Sun, Microwave-assisted synthesis of CdS-reduced graphene oxide composites for photocatalytic reduction of Cr(VI), Chem. Commun. 47 (2011) 11984–11986.

[10] Y.C. Zhang, J. Li, M. Zhang, D.D. Dionysiou, Size-tunable hydrothermal synthesis of SnS_2 nanocrystals with high performance in visible light-driven photocatalytic reduction of aqueous Cr(VI), Environ. Sci. Technol. 45 (21) (2011) 9324–9331.

[11] W. Yang, L. Zhang, Y. Hu, Y. Zhong, H.B. Wu, X.W. Lou, Microwave-assisted synthesis of porous Ag_2S-Ag hybrid nanotubes with high visible-light photocatalytic activity, Angew. Chem. Int. Ed. 51 (2012) 11501–11504.

[12] X.-D. Du, X.-H. Yi, P. Wang, W. Zheng, J. Deng, C.-C. Wang, Robust photocatalytic reduction of Cr(VI) on UiO-66-NH_2(Zr/Hf) metal-organic framework membrane under sunlight irradiation, Chem. Eng. J. 356 (2019) 393–399.

[13] X.-H. Yi, S.-Q. Ma, X.-D. Du, C. Zhao, H. Fu, P. Wang, C.-C. Wang, The facile fabrication of 2D/3D Z-scheme g-C_3N_4/UiO-66 heterojunction with enhanced photocatalytic Cr(VI) reduction performance under white light, Chem. Eng. J. 375 (2019), 121944.

[14] S. Deiana, A. Premoli, C. Senette, Reduction of Cr(VI) by caffeic acid, Chemosphere 67 (10) (2007) 1919–1926.

[15] Y.-H. Li, X.-H. Yi, Y.-X. Li, C.-C. Wang, P. Wang, C. Zhao, W. Zheng, Robust Cr(VI) reduction over hydroxyl modified UiO-66 photocatalyst constructed from mixed ligands: Performances and mechanism insight with or without tartaric acid, Environ. Res. 201 (2021), 111596.

[16] X.-R. Xu, H.-B. Li, X.-Y. Li, J.-D. Gu, Reduction of hexavalent chromium by ascorbic acid in aqueous solutions, Chemosphere 57 (7) (2004) 609–613.

[17] Z. Xu, S. Bai, J. Liang, L. Zhou, Y. Lan, Photocatalytic reduction of Cr(VI) by citric and oxalic acids over biogenetic jarosite, Mater. Sci. Eng. C 33 (4) (2013) 2192–2196.

[18] H. Zhang, P. Zhang, K. Ye, Y. Sun, S. Jiang, Y. Wang, W. Pang, Mesoporous material grafted with luminescent molecules for the design of selective metal ion chemosensor, J. Lumin. 117 (2006) 68–74.

[19] M. Li, I. Katsouras, C. Piliego, G. Glasser, I. Lieberwirth, P.W.M. Blom, D.M. de Leeuw, Controlling the microstructure of poly(vinylidene-fluoride) (PVDF) thin films for microelectronics, J. Mater. Chem. C 1 (2013) 7695–7702.

[20] K. Schneider, M. Lubecka, A. Czapla, V_2O_5 thin films for gas sensor applications, Sens. Actuators B Chem. 236 (2016) 970–977.

[21] J. Gascon, F. Kapteijn, Metal-organic framework membranes–high potential, bright future? Angew. Chem. Int. Ed. 49 (2010) 1530–1532.

[22] Y. Sun, F. Yang, Q. Wei, N. Wang, X. Qin, S. Zhang, B. Wang, Z. Nie, S. Ji, H. Yan, J. R. Li, Oriented Nano-Microstructure-Assisted Controllable Fabrication of Metal-Organic Framework Membranes on Nickel Foam, Adv. Mater. 28 (2016) 2374–2381.

[23] K. Shqau, M.L. Mottern, D.i. Yu, H. Verweij, Preparation and Properties of Porous alpha-Al_2O_3 Membrane Supports, J. Am. Ceram. Soc. 89 (6) (2006) 1790–1794, https://doi.org/10.1111/j.1551-2916.2006.01037.x.

[24] Y. Hu, X. Dong, J. Nan, W. Jin, X. Ren, N. Xu, Y.M. Lee, Metal-organic framework membranes fabricated via reactive seeding, Chem. Commun. 47 (2011) 737–739.

[25] M.A.G.J.J. Testa, M.I. Litter, Experimental Evidence in Favor of an Initial One-Electron-Transfer Process in the Heterogeneous Photocatalytic Reduction of Chromium(VI) over TiO_2, Langmuir 17 (2001) 3515.

[26] C. Athanasekou, G.E. Romanos, S.K. Papageorgiou, G.K. Manolis, F. Katsaros, P. Falaras, Photocatalytic degradation of hexavalent chromium emerging contaminant via advanced titanium dioxide nanostructures, Chem. Eng. J. 318 (2017) 171–180.

[27] G. Velegraki, J. Miao, C. Drivas, B. Liu, S. Kennou, G.S. Armatas, Fabrication of 3D mesoporous networks of assembled CoO nanoparticles for efficient photocatalytic reduction of aqueous Cr(VI), Appl. Catal. B 221 (2018) 635–644.

[28] P.-C. Yu, Y.-W. Tsai, F.-S. Yen, C.-L. Huang, W.C. Wei, Thermal Reaction of Cristobalite in Nano-SiO_2/α-Al_2O_3 Powder Systems for Mullite Synthesis, J. Am. Ceram. Soc. 97 (2014) 2431–2438.

[29] A. Moses Ezhil Raj, S.G. Victoria, V.B. Jothy, C. Ravidhas, J. Wollschläger, M. Suendorf, M. Neumann, M. Jayachandran, C. Sanjeeviraja, XRD and XPS characterization of mixed valence Mn_3O_4 hausmannite thin films prepared by chemical spray pyrolysis technique, Appl. Surf. Sci. 256 (9) (2010) 2920–2926.

[30] L. Castro, R. Dedryvère, J.B. Ledeuil, J. Bréger, C. Tessier, D. Gonbeau, Aging Mechanisms of $LiFePO_4$//Graphite Cells Studied by XPS: Redox Reaction and Electrode/Electrolyte Interfaces, J. Electrochem. Soc. 159 (2012) A357–A363.

[31] Z. Zhang, X. Li, B. Liu, Q. Zhao, G. Chen, Hexagonal microspindle of NH_2-MIL-101 (Fe) metal–organic frameworks with visible-light-induced photocatalytic activity for the degradation of toluene, RSC Adv. 6 (2016) 4289–4295.

[32] X.-H. Yi, H. Ji, C.-C. Wang, Y. Li, Y.-H. Li, C. Zhao, A. Wang, H. Fu, P. Wang, X. Zhao, W. Liu, Photocatalysis-activated SR-AOP over PDINH/MIL-88A(Fe) composites for boosted chloroquine phosphate degradation: Performance, mechanism, pathway and DFT calculations, Appl. Catal. B 293 (2021), 120229.

[33] G. Mattogno, G. Righini, G. Montesperelli, E. Traversa, XPS analysis of the interface of ceramic thin films for humidity sensors, Appl. Surf. Sci. 70–71 (1993) 363–366.

[34] D. Jin, J. Gao, Z. Hou, Y. Guo, X. Lu, Y. Zhu, X. Zheng, Microwave assisted in situ synthesis of USY-encapsulated heteropoly acid (HPW-USY) catalysts, Appl. Catal. A: Gen. 352 (2009) 259–264.

[35] B. Liu, Y. Wu, X. Han, J. Lv, J. Zhang, H. Shi, Facile synthesis of g-C_3N_4/amine-functionalized MIL-101(Fe) composites with efficient photocatalytic activities under visible light irradiation, J. Mater. Sci. Mater. Electron. 29 (2018) 17591–17601.

[36] L.i. Shi, T. Wang, H. Zhang, K. Chang, X. Meng, H. Liu, J. Ye, An Amine-Functionalized Iron(III) Metal-Organic Framework as Efficient Visible-Light Photocatalyst for Cr(VI) Reduction, Adv. Sci. 2 (3) (2015) 1500006, https://doi.org/10.1002/advs.201500006.

[37] P. Li, M. Guo, Q. Wang, Z. Li, C. Wang, N. Chen, C.-C. Wang, C. Wan, S. Chen, Controllable synthesis of cerium zirconium oxide nanocomposites and their application for photocatalytic degradation of sulfonamides, Appl. Catal. B 259 (2019), 118107.

[38] S. Ouyang, J. Ye, β-AgAl1-x$GaxO_2$ Solid-Solution Photocatalysts: Continuous Modulation of Electronic Structure toward High-Performance Visible-Light Photoactivity, J. Am. Chem. Soc. 133 (20) (2011) 7757–7763, https://doi.org/10.1021/ja110691t.

[39] N. Wang, L. Zhu, K. Deng, Y. She, Y. Yu, H. Tang, Visible light photocatalytic reduction of Cr(VI) on TiO_2 in situ modified with small molecular weight organic acids, Appl. Catal. B 95 (3-4) (2010) 400–407, https://doi.org/10.1016/j.apcatb.2010.01.019.

[40] H. Peng, J. Guo, Reduction behavior of chromium(VI) with oxalic acid in aqueous solution, Sci. Rep. 10 (2020) 17732, https://doi.org/10.1038/s41598-020-74928-7.

[41] A.U. Chaudhari, S.R. Tapase, V.L. Markad, K.M. Kodam, Simultaneous decolorization of reactive Orange M2R dye and reduction of chromate by Lysinibacillus sp. KMK-A, J. Hazard. Mater. 262 (2013) 580–588.

[42] F. Zhang, Y. Zhang, C. Zhou, Z. Yang, H. Xue, D.D. Dionysiou, A new high efficiency visible-light photocatalyst made of SnS_2 and conjugated derivative of polyvinyl alcohol and its application to Cr(VI) reduction, Chem. Eng. J. 324 (2017) 140–153.

[43] F. Zhang, Y. Zhang, G. Zhang, Z. Yang, D.D. Dionysiou, A. Zhu, Exceptional synergistic enhancement of the photocatalytic activity of SnS_2 by coupling with polyaniline and N-doped reduced graphene oxide, Appl. Catal. B 236 (2018) 53–63.

[44] H. He, Q.i. Sun, W. Gao, J.A. Perman, F. Sun, G. Zhu, B. Aguila, K. Forrest, B. Space, S. Ma, A Stable Metal-Organic Framework Featuring a Local Buffer Environment for Carbon Dioxide Fixation, Angew. Chem. Int. Ed. 57 (17) (2018) 4657–4662, https://doi.org/10.1002/anie.v57.1710.1002/anie.201801122.

[45] M. Gheju, A. Iovi, Kinetics of hexavalent chromium reduction by scrap iron, J. Hazard. Mater. 135 (1) (2006) 66–73.

[46] M. Naimi-Joubani, M. Shirzad-Siboni, J.-K. Yang, M. Gholami, M. Farzadkia, Photocatalytic reduction of hexavalent chromium with illuminated ZnO/TiO_2 composite, J. Ind. Eng. Chem. 22 (2015) 317–323.

[47] C. Wang, L. Zhu, M. Wei, P. Chen, G. Shan, Photolytic reaction mechanism and impacts of coexisting substances on photodegradation of bisphenol A by Bi_2WO_6 in water, Water Res. 46 (2012) 845–853.

[48] F. Martínez, J.A. Melero, J.Á. Botas, M.I. Pariente, R. Molina, Treatment of Phenolic Effluents by Catalytic Wet Hydrogen Peroxide Oxidation over Fe_2O_3/SBA-15 Extruded Catalyst in a Fixed-Bed Reactor, Ind. Eng. Chem. Res. 46 (13) (2007) 4396–4405.

[49] L. Ju, P. Wu, X. Lai, S. Yang, B. Gong, M. Chen, N. Zhu, Synthesis and characterization of Fullerene modified ZnAlTi-LDO in photo-degradation of Bisphenol A under simulated visible light irradiation, Environ. Pollut. 228 (2017) 234–244.

[50] G. Dong, L. Zhang, Synthesis and Enhanced Cr(VI) Photoreduction Property of Formate Anion Containing Graphitic Carbon Nitride, J. Phys. Chem. A 117 (8) (2013) 4062–4068.

[51] J.C. Wang, J. Ren, H.C. Yao, L. Zhang, J.S. Wang, S.Q. Zang, L.F. Han, Z.J. Li, Synergistic photocatalysis of Cr(VI) reduction and 4-Chlorophenol degradation over hydroxylated alpha-Fe_2O_3 under visible light irradiation, J. Hazard. Mater. 311 (2016) 11–19.

[52] F. Villamena, E. Locigno, A. Rockenbauer, C. Hadad, J. Zweier, Theoretical and Experimental Studies of the Spin Trapping of Inorganic Radicals by 5,5-Dimethyl-1-Pyrroline N -Oxide (DMPO). 2. Carbonate Radical Anion, J. Phys. Chem. A 111 (2007) 384-391. https://doi.org/10.1021/jp065692d.

[53] H. Ren, Z. Hou, X. Han, R. Zhou, Highly reductive radical $CO_2^{\bullet-}$deriving from a system with $SO_4^{\bullet-}$and formate anion: Implication for reduction of Cr(VI) from wastewater, Chem. Eng. J. 309 (2017) 638–645.

[54] F. Zhao, Y. Liu, S.B. Hammouda, B. Doshi, N. Guijarro, X. Min, C.-J. Tang, M. Sillanpää, K. Sivula, S. Wang, MIL-101(Fe)/g-C3N4 for enhanced visible-light-driven photocatalysis toward simultaneous reduction of Cr(VI) and oxidation of bisphenol A in aqueous media, Appl. Catal. B 272 (2020), 119033.

[55] L. Zhang, F. Cao, J. Sun, Y. Sun, The synergistic effect of attapulgite in the highly enhanced photoreduction of Cr(VI) by oxalic acid in aqueous solution, Environ Res 197 (2021) 111070, https://doi.org/10.1016/j.envres.2021.111070.

[56] V.K. Sharma, M. Feng, Water depollution using metal-organic frameworks-catalyzed advanced oxidation processes: A review, J. Hazard. Mater. 372 (2019) 3–16.

[57] Y. AlSalka, O. Al-Madanat, M. Curti, A. Hakki, D.W. Bahnemann, Photocatalytic H_2 Evolution from Oxalic Acid: Effect of Co-catalysts and Carbon Dioxide Radical Anion on the Surface Charge Transfer Mechanisms, ACS Appl. Energy Mater. 3 (7) (2020) 6678–6691, https://doi.org/10.1021/acsaem.0c00826.

[58] L. Zhang, J. Sun, W. Niu, F. Cao, The synergetic role of rice straw in enhancing the process of Cr(VI) photoreduction by oxalic acid, Environ. Pollut. 265 (2020), 115013.

[59] X. Liu, G. Liu, S. You, Effective in-situ reduction of Cr(VI) from leather wastewater by advanced reduction process based on /$CO_2^{\bullet-}$/ with visible-light photocatalyst, Chemosphere 263 (2021), 127898.